Journal of Optics

PAPER

High-conductivity silicon based spectrally selective plasmonic surfaces for sensing in the infrared region

To cite this article: K Gorgulu *et al* 2017 *J. Opt.* **19** 025002

IOP Publishing Journal of Optics
J. Opt. 19 (2017) 025002 (6pp) doi:10.1088/2040-8986/19/2/025002

High-conductivity silicon based spectrally selective plasmonic surfaces for sensing in the infrared region

K Gorgulu[1,4], A Gok[1,4], M Yilmaz[2], K Topalli[2,3,5] and A K Okyay[1,2,3,5,]

[1] Department of Electrical and Electronics Engineering, Bilkent University, Ankara 06800, Turkey
[2] UNAM-National Nanotechnology Research Center, Bilkent University, Ankara 06800, Turkey
[3] Institute of Materials Science and Nanotechnology, Bilkent University, Ankara 06800, Turkey

E-mail: aokyay@stanfordalumni.org

Received 23 September 2016, revised 5 November 2016
Accepted for publication 18 November 2016
Published 30 December 2016

Abstract

Plasmonic perfect absorbers have found a wide range of applications in imaging, sensing, and light harvesting and emitting devices. Traditionally, metals are used to implement plasmonic structures. For sensing applications, it is desirable to integrate nanophotonic active surfaces with biasing and amplification circuitry to achieve monolithic low cost solutions. Commonly used plasmonic metals such as Au and Ag are not compatible with standard silicon complementary metal–oxide–semiconductor (CMOS) technology. Here we demonstrate plasmonic perfect absorbers based on high conductivity silicon. Standard optical lithography and reactive ion etching techniques were used for the patterning of the samples. We present computational and experimental results of surface plasmon resonances excited on a silicon surface at normal and oblique incidences. We experimentally demonstrate our absorbers as ultra-low cost, CMOS-compatible and efficient refractive index sensing surfaces. The experimental results reveal that the structure exhibits a sensitivity of around 11 000 nm/RIU and a figure of merit of up to 2.5. We also show that the sensing performance of the structure can be improved by increasing doping density.

Keywords: plasmonics, absorber, infrared, refractive index sensing, silicon

(Some figures may appear in colour only in the online journal)

1. Introduction

Plasmonic and metamaterial electromagnetic absorbers have attracted extensive attention not only for their fascinating electromagnetic properties, but also for their potential for various photonic applications. A perfect absorber absorbs all incident radiation at the frequency of operation by suppressing reflection, transmission and scattering in the structure. The first studies on metamaterial absorbers were in the microwave and THz regimes, utilizing two metallic layers separated by a dielectric layer [1–3]. Perfect absorption has been demonstrated with different types of unit cell structures such as patches, stripes and discs at these wavelengths. A downscaling of unit cell dimensions allowed practical perfect absorbers at mid-infrared, near infrared and visible wavelengths with very high absorption efficiencies [4–6].

Carefully designed sub-wavelength metallic structures provide excitation of plasmonic and photonic resonances that show narrow absorption bands. Researchers tried to increase the absorption waveband by exploiting multiple resonances simultaneously, for applications where broadband absorption is desirable [7, 8]. However, some other applications, such as selective thermal emitters and detectors, and bio-chemical and refractive index sensors, require narrow absorption bands [9, 10]. Plasmonic absorbers typically have narrow resonance bands and therefore they can be utilized in spectrally selective

[4] These authors contributed equally.
[5] Dr Okyay and Dr Topalli were with Bilkent University at the time of the study.

detection schemes such as uncooled microbolometers [8]. According to Kirchhoff's law of thermal radiation, a perfect absorber is equivalent to a good thermal emitter. In order to get a sharp emissivity peak, a narrowband absorber is required. Narrow resonance bands are also highly desirable in sensing applications in order to detect minute changes in the environment. Plasmonic resonances, confined to a metal dielectric surface, are extremely sensitive to the refractive index of the surrounding dielectric medium. Such strong dependency on the refractive index of the surrounding dielectric medium paves the way for ultra-sensitive label-free refractive index sensing applications [11, 12].

All examples mentioned above utilize conventional metallic components, such as gold and silver, as their material building blocks. In commonly used metals, the magnitude of the real part of the permittivity is very large at mid-infrared wavelengths. This feature of metals significantly limits their plasmonic mode confinement in the mid-infrared regime [13]. Conventional metals such as Ag also pose fabrication challenges and have degradation problems on exposure to air or humidity, limiting fabrication and integration of devices [14]. On the other hand, highly doped semiconductors are shown to exhibit plasmonic behavior in the mid-infrared regime [15–19]. Compared to their metallic counterparts, highly doped semiconductors provide enhanced device performance, and fabrication and CMOS integration feasibility. Due to silicon's prevailing manufacturing knowledge base, silicon plasmonics has received great attention. Localized surface plasmon resonances excited on silicon nanowires synthesized via the vapor–liquid–solid technique have been demonstrated [20]. Infrared absorption performance of a one-dimensional (1D) silicon grating and its possible application as a biological sensor have been studied computationally [21, 22]. Also, surface plasmon based thermal emission from patterned silicon has been studied experimentally [23].

In this paper we numerically and experimentally demonstrate frequency selective infrared absorbers based on highly conductive silicon (p-type, $\rho = 0.001$–$0.002\ \Omega\,\mathrm{cm}$). Furthermore, we demonstrate that the designed plasmonic devices are promising as efficient refractive index based sensing surfaces. We also study the dependence of sensing performance of our structure on the doping concentration of silicon.

2. Structure and methods

Figure 1(a) presents a schematic representation of the proposed structures. Two-dimensional (2D) grating structures were patterned on a highly conductive silicon wafer using standard photolithography and reactive ion etching (RIE) techniques. First, we spun a photoresist, AZ 5214E at 4000 rpm, and baked it at 110 °C for 50 s. Then, we exposed the photoresist to a contact aligner and developed the photoresist with a deionized water diluted AZ 400 K developer. Silicon was patterned using a BOSCH process recipe that is SF_6 based RIE at the etch step, and C_4F_8 based deposition at the passivation step. Then, the remaining photoresist was

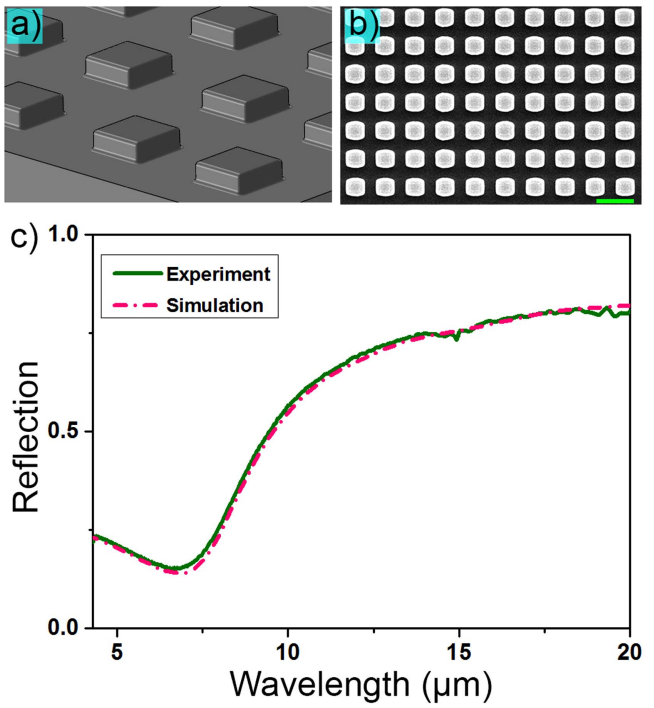

Figure 1. (a) Schematic illustration of 2D grating structures. (b) Top-view scanning electron microscope image of the 2D plasmonic absorber structure with periodicity of $P = 8\ \mu$m and fill ratio of 0.65. Scale bar is 10 μm. (c) Measured and simulated reflection from the flat silicon surface.

removed by an oxygen plasma cleaning recipe. Two structures with different periodicities, $P = 8\ \mu$m and $P = 9\ \mu$m, and different widths, $W = 5.2\ \mu$m and $W = 5.85\ \mu$m, were made. The height of the gratings is $1.4\ \mu$m. A top view scanning electron microscope (SEM) image of the 2D silicon absorber with periodicity $P = 8\ \mu$m is shown in figure 1(b). Reflection spectra from the fabricated samples were obtained using a Bruker HYPERION IR microscope and Bruker Vertex 70v Fourier transform infrared (FTIR) spectrometer with a gold mirror as the calibration reference.

Optical properties of the highly conductive silicon can be modeled using the Drude formalism considering carrier density and mobility as the fitting parameters of the material [24, 25]. According to the model, carrier density and mobility of highly doped silicon used in this study were $7.5 \times 10^{19}\ \mathrm{cm}^{-3}$ and $51\ \mathrm{cm}^2\ \mathrm{V}^{-1}\ \mathrm{s}^{-1}$, respectively. There is a characteristic transition wavelength called plasma wavelength which is defined as the wavelength at which the real part of the permittivity vanishes. The plasma wavelength of highly doped silicon substrates used in this study was calculated to be $\lambda_{pl} = 8.2\ \mu$m. At wavelengths longer than the plasma wavelength, the real part of permittivity becomes negative and highly doped silicon behaves like a metal. Therefore, surface plasmons can be excited in this regime.

Electromagnetic wave simulations were performed using the finite difference time domain (FDTD) method by Lumerical Inc., a commercially available FDTD simulation software package. A three dimensional (3D) simulation setup is used; on the x and y axes periodic boundary conditions are

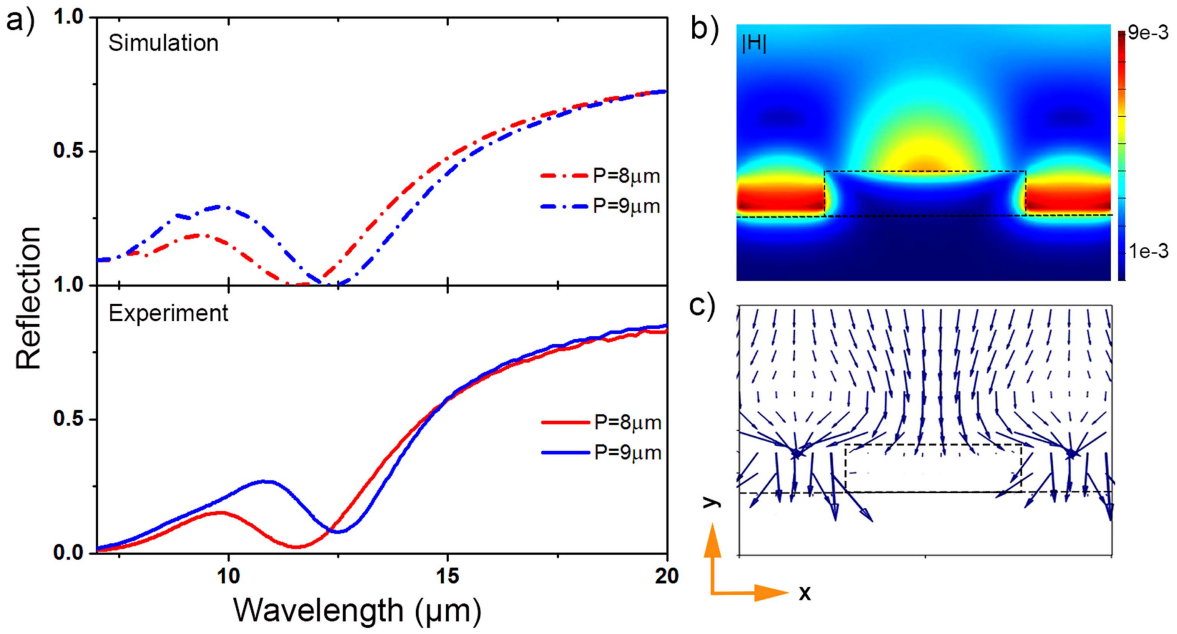

Figure 2. (a) Simulated and measured reflection spectra for structures with periodicities of $P = 8\ \mu$m and $P = 9\ \mu$m, and fill ratio of 0.65 for both structures. (b) Cross section of the time-averaged magnetic field for the structure with periodicity $P = 9\ \mu$m at the resonance wavelength. (c) Cross section of the time-averaged optical power flow vector distribution.

used. On the z-axis (propagation direction) a perfectly matched layer (PML) is used. In all of the simulations, we employ a cubic mesh with a mesh size of 10 nm.

We performed simulations and experiments for the reflection behavior of a flat silicon surface. The reflectance results from the simulation and experiment for a flat surface are given in figure 1(c). The simulation result and experimental measurement are in good agreement. The reflection results presented in figure 1(c) are also confirmed by analytical reflection calculations obtained by Fresnel's equation.

3. Results and discussion

3D structures used in the FDTD simulations were imported from digitized SEM images of experimentally obtained 2D gratings. Figure 2(a) shows the calculated and measured reflection spectra of the 2D plasmonic absorber structures for arbitrarily polarized light at normal incidence in the wavelength range from 7 μm to 20 μm. The 2D surface pattern gives a polarization insensitive optical response. The measured reflection spectrum for the 2D grating with period $P = 8\ \mu$m shows approximately 98% absorption at the resonance wavelength. Such a near perfect absorption can be ascribed to efficient coupling of incident light into surface plasmon modes through momentum matching by diffraction. Considering normal incidence, in such grating structures the plasmon wavevector, k_x, is generally determined by the Bragg vectors associated with the grating periodicities. However, because the structure dimensions are close to the wavelength of operation, resonance wavelength can be modified by the height and width of the gratings. As reported in a previous study, increasing the height of the grating leads to redshift in the resonance wavelength [23]. Structures with grating periodicities of 8 μm and 9 μm have reflection dips at 11.5 μm and 12.5 μm, respectively. Figure 2(b) shows a time-averaged magnetic field map for the structure with periodicity $P = 9\ \mu$m at the resonance wavelength. As shown in the figure, magnetic field is strongly concentrated within the air trench surrounded by three highly doped silicon–air interfaces. Figure 2(c) shows the time-averaged power flow distribution. The excitation of plasmonic resonance allows penetration of light into highly doped silicon and leads to strong optical absorption.

Angular reflection measurements were obtained using a J A Woollam IR-Vase spectroscopic ellipsometer. The optical response of the plasmonic absorbers for different angles of incidence were also calculated with the FDTD technique. Figure 3 shows the reflection spectra for a 1D periodic sample in the case of three different angles of incidence. Simulated (dashed lines) reflectance spectra for the structures are in spectral agreement with experimental results (solid lines), but there are amplitude variations between measurement and experiment. For the simple 1D grating of grooves, phase-matching takes place whenever the condition $\beta = k\sin\theta \pm \nu k_x$ is fulfilled, where k is the wavevector of the light incident at an angle θ, and $\nu = (1, 2, 3\ldots)$. Therefore, increasing the angle of incidence redshifts the resonance wavelength. When the period increases, the effect of the reciprocal vector reduces. Hence, angular sensitivity increases with increasing structure period.

We investigated the refractive index sensitivity of our plasmonic absorber structures by immersing the structure with periodicity $P = 9\ \mu$m in acetone and measuring the reflection spectrum. In the sensing experiments, the liquid film thickness of acetone is about 200 μm (which is much greater than

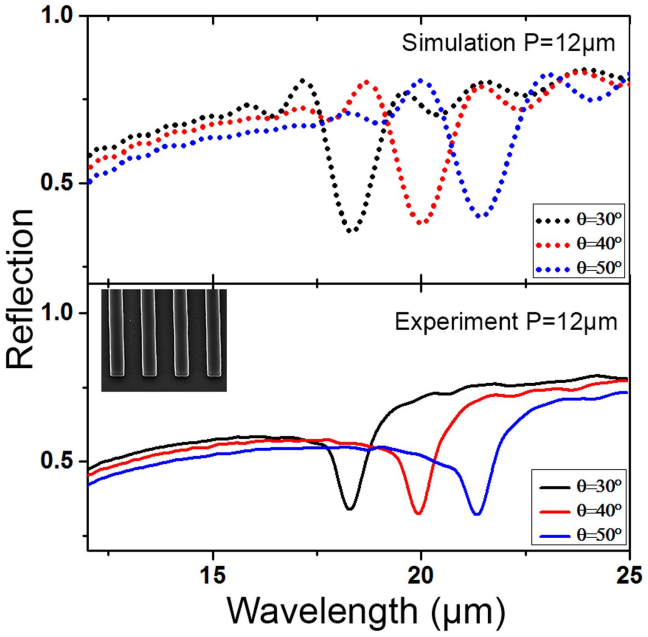

Figure 3. Simulated and measured reflection spectra at three different incidence angles for the structure with $P = 12\ \mu$m, fill ratio of 0.45 and height of 1.4 μm. The inset shows the fabricated 1D device structure.

the penetration depth of surface plasmons into the material above the silicon surface [19]). The sensitivity of a surface plasmon resonance based sensor is defined as the change in resonant wavelength as a function of change in refractive index, $S = \Delta\lambda/\Delta n$ nm/RIU. Since it is easier to detect resonance changes with narrow lines, the sensitivity is divided into full-width at half-maximum (FWHM) to determine the figure of merit, FOM = S/FWHM. Figure 4(a) shows reflection spectra for the same structure in two different media, air and acetone, and the infrared reflection spectrum of acetone. The refractive index of acetone is taken as 1.35 [26]. However, acetone has several molecular resonances over the entire mid-infrared region and the refractive index of acetone is modified in the vicinity of these resonance regions. In order to eliminate the effect of these resonances, reflection measurements of the plasmonic absorber under acetone are normalized to the infrared reflection spectrum of pure acetone. After normalization, molecular resonances of acetone are alleviated but they are still discernable in the spectrum. However, line-widths of these resonances are much smaller than the line-widths of the plasmonic resonances. Therefore, plasmonic (indicated by blue arrows) and molecular (indicated by red arrows) resonances can be distinguished easily. We also simulated the reflection spectra for different refractive indices of the surrounding medium (figure 4(b)). As depicted in figure 4(b), the reflection spectrum shows a gradual redshift with increasing refractive index values. Both measured and simulated resonance wavelengths as a function of refractive index of the surrounding medium are given in figure 4(c). According to the linear fitting of the resonance frequencies, the sensitivity value is found to be approximately 11 000 nm/RIU. Using this sensitivity value, the FOM value is calculated as 2.5. In general, the sensitivity of refractive index sensors is proportional to the operation wavelength. Therefore, the sensitivity of our absorber is very high compared to previous studies presenting their results at visible or near infrared regions [10, 12, 27–29]. However, in order to have a high FOM, the line-width of the resonance should be as small as possible. Even if our absorber has improved sensitivity, it has relatively low FOM values compared to the literature. It is important to note that reports of refractive index sensing applications on using conventional metals typically utilize either e-beam lithography or focused ion beam patterning. These techniques are costly and time-consuming for the fabrication of large-scale structures. Therefore, 1X contact photolithography and reduction photolithography based wafer scale fabrication of our silicon based sensors are promising for cost-effective applications.

The real and imaginary parts of dielectric permittivity of a semiconductor increase with doping concentration. Therefore, optical properties of a semiconductor become similar to those of traditional metals as the impurity concentration increases. We extracted optical properties of doped silicon

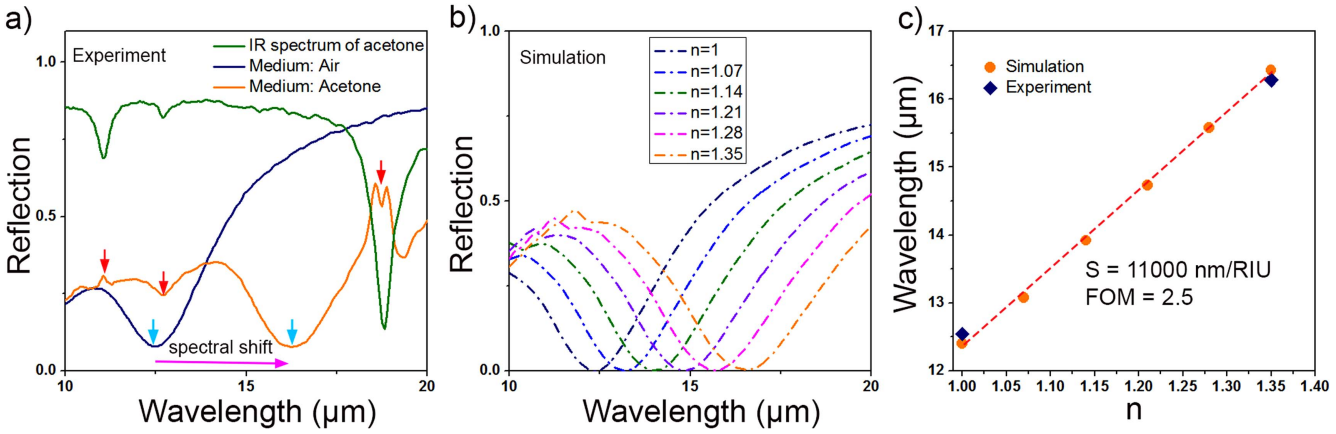

Figure 4. (a) Measured reflection spectra of the structure with periodicity $P = 9\ \mu$m in two different media. Red arrows show the molecular resonance points of the acetone. Blue arrows show the plasmonic resonances of the patterned silicon under air and acetone. (b) Simulated reflection spectra for different refractive indices of the surrounding medium. (c) Measured and simulated resonance wavelengths as a function of refractive index of the surrounding medium.

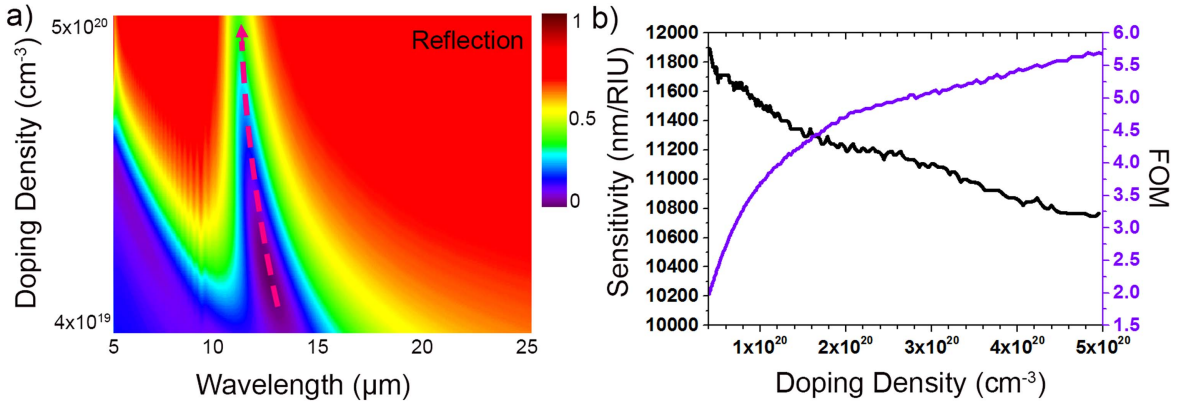

Figure 5. Reflection spectrum as a function of doping density for the structure with periodicity $P = 9$ μm and fill ratio of 0.65. (b) Calculated sensitivity and FOM as a function of doping density.

using the Drude formalism for doping values from $4 \times 10^{19}\,\mathrm{cm}^{-3}$ to $5 \times 10^{20}\,\mathrm{cm}^{-3}$. We considered the dependence of mobility on the carrier concentration in calculations of the optical constants [30]. We investigated the dependence of the sensing performance on the doping density of silicon. We performed FDTD simulations for the same structure with different doping densities and two different refractive indices of the surrounding medium, $n = 1$ and $n = 1.2$. Figure 5(a) shows the simulated reflection spectrum as a function of doping density for the structure with air as the surrounding medium. As is seen in the figure, as the doping density increases, the resonance band becomes narrower and resonance wavelength shifts to shorter wavelengths (indicated by the dashed line). As the doping concentration increases, the plasma frequency shifts to shorter wavelengths, surface plasmon dispersion curves also shift to higher frequencies. Figure 5(b) shows the sensitivity and FOM as a function of doping density. There is no significant change in the sensitivity, but the FOM increases with increasing doping density. As the doping concentration increases, the imaginary part of the dielectric function increases and the loss tangent decreases. These changes in the optical properties make the resonance band narrower [31], thus FOM and the sensing quality increase. A FOM value of 5.7 is obtained when the doping density is $5 \times 10^{20}\,\mathrm{cm}^{-3}$, and this value is greater or comparable to previously reported values obtained from various plasmonic structures [28, 32, 33].

4. Conclusion

In summary, we have demonstrated all-silicon plasmonic absorbers with excellent absorption performances. Periodic silicon gratings were fabricated by scalable and cost effective methods including conventional photolithography and reactive ion etching techniques. We showed the spectral dependence of the resonance wavelength on the period of the structure and we studied the incidence angle behavior of the resonance wavelength. We further demonstrated the refractive index capability of silicon absorbers and showed a sensitivity of 11 000 nm/RIU and FOM value of 2.5. We also showed that the resonance waveband decreases as the doping density increases, thus sensing quality increases. In light of their ease of fabrication, silicon based plasmonic absorbers are highly advantageous for refractive index sensors.

Acknowledgments

This work was partially supported by the Scientific and Technological Research Council of Turkey (TUBITAK) under Grant Nos. 112M004, 112E052, and 113M815. A K O acknowledges support from the Turkish Academy of Sciences Distinguished Young Scientist Award (TUBA GEBIP), BAGEP Award and FABED Award. K G and A G thank TUBITAK-BIDEB for MS scholarship.

References

[1] Landy N I, Sajuyigbe S, Mock J J, Smith D R and Padilla W J 2008 *Phys. Rev. Lett.* **100** 207402
[2] Wang B, Koschny T and Soukoulis C M 2009 *Phys. Rev.* B **803** 033108
[3] Tao H, Bingham C M, Strikwerda A C, Pilon D, Shrekenhamer D, Landy N I and Averitt R D 2008 *Phys. Rev.* B **782** 241103
[4] Hedayati M K, Javaherirahim M, Mozooni B, Abdelaziz R, Tavassolizadeh A, Chakravadhanula V S K, Zaporojtchenko V, Strunkus T, Faupel F and Elbahri M 2011 *Adv. Mater.* **23** 5410–4
[5] Teperik T V, De Abajo F G, Borisov A G, Abdelsalam M, Bartlett P N, Sugawara Y and Baumberg J J 2008 *Nat. Photon.* **25** 299–301
[6] Yao Y, Shankar R, Kats M A, Song Y, Kong J, Loncar M and Capasso F 2014 *Nano Lett.* **1411** 6526–32
[7] Aydin K, Ferry V E, Briggs R M and Atwater H A 2011 *Nat. Commun.* **2** 517
[8] Watts C M, Liu X and Padilla W J 2012 *Adv. Mater.* **24** OP98–OP120
[9] Tittl A, Mai P, Taubert R, Dregely D, Liu N and Giessen H 2011 *Nano Lett.* **1110** 4366–9
[10] Liu N, Mesch M, Weiss T, Hentschel M and Giessen H 2010 *Nano Lett.* **107** 2342–8
[11] Adato R and Altug H 2013 *Nat. Commun.* **4** 2154

[12] Shen Y, Zhou J, Liu T, Tao Y, Jiang R, Liu M and Jin C 2013 *Nat. Commun.* **4** 2381
[13] Zhong Y, Malagari S D, Hamilton T and Wasserman D 2015 *Nanophotonics* **91** 093791
[14] Naik G V, Shalaev V M and Boltasseva A 2013 *Adv. Mater.* **2524** 3264–94
[15] Law S, Adams D C, Taylor A M and Wasserman D 2012 *Opt. Express* **2011** 12155–65
[16] Jung J and Pedersen T G 2013 *J. Appl. Phys.* **113** 114904
[17] Law S, Yu L, Rosenberg A and Wasserman D 2013 *Nano Lett.* **13** 4569–74
[18] Zhong Y, Malagari S D, Hamilton T and Wasserman D 2015 *J. Nanophoton.* **91** 093791
[19] Shahzad M, Medhi G, Peale R E, Buchwald W R, Cleary J W, Soref R and Edwards O 2011 *J. Appl. Phys.* **11012** 123105
[20] Chou L W, Shin N, Sivaram S V and Filler M A 2012 *J. Am. Chem. Soc.* **13439** 16155–8
[21] Chen Y B and Zhang Z M 2008 *J. Phys. D: Appl. Phys.* **41** 095406
[22] Chen Y B 2009 *Opt. Express* **17** 3130–40
[23] Ribaudo T, Peters D W, Ellis A R, Davids P S and Shaner E A 2013 *Opt. Express* **216** 6837–44
[24] Gok A, Yilmaz M, Bıyıklı N, Topallı K and Okyay A K 2016 *J. Opt.* **18** 035002
[25] Cleary J W, Peale R E, Shelton D J, Boreman G D, Smith C W, Ishigami M and Buchwald W R 2010 *J. Opt. Soc. Am.* B **274** 730–4
[26] Iglesias M, Orge B and Tojo J 1996 *Fluid Phase Equilib.* **1262** 203–23
[27] Cheng F, Yang X and Gao J 2014 *Opt. Lett.* **3911** 3185–8
[28] Pryce I M, Kelaita Y A, Aydin K and Atwater H A 2011 *ACS Nano* **510** 8167–74
[29] Cetin A E, Etezadi D, Galarreta B C, Busson M P, Eksioglu Y and Altug H 2015 *ACS Photon.* **28** 1167–74
[30] Basu S, Lee B J and Zhang Z M 2010 *J. Heat Transfer* **132** 023301
[31] Singh R, Azad A K, O'Hara J F, Taylor A J and Zhang W 2008 *Opt. Lett.* **3313** 1506–8
[32] Gu Y, Li Q, Xiao J, Wu K and Wang G P 2011 *J. Appl. Phys.* **1092** 023104
[33] Mandal P 2015 *Plasmonics* **102** 439–45